NANO LETTERS

Letter

pubs.acs.org/NanoLett

Direct Atomic-Level Observation and Chemical Analysis of ZnSe Synthesized by *in Situ* High-Throughput Reactive Fiber Drawing

Chong Hou,[†,‡,§] Xiaoting Jia,[‡,§] Lei Wei,[‡,§] Alexander M. Stolyarov,[‡,§] Ofer Shapira,[‡,§,†] John D. Joannopoulos,[‡,§,∥] and Yoel Fink*[,†,‡,§,⊥]

[†]Department of Materials Science and Engineering, Massachusetts Institute of Technology, Cambridge, Massachusetts 02139, United States

[‡]Institute of Soldier Nanotechnology, Massachusetts Institute of Technology, Cambridge, Massachusetts 02139, United States

[§]Research Laboratory of Electronics, Massachusetts Institute of Technology, Cambridge, Massachusetts 02139, United States

[⊥]Department of Electrical Engineering and Computer Science, Massachusetts Institute of Technology, Cambridge, Massachusetts 02139, United States

[∥]Department of Physics, Massachusetts Institute of Technology, Cambridge, Massachusetts 02139, United States

Supporting Information

ABSTRACT: We demonstrate a high-throughput method for synthesizing zinc selenide (ZnSe) *in situ* during fiber drawing. Central to this method is a thermally activated chemical reaction occurring across multiple interfaces between alternately layered elemental zinc- (Zn-) and selenium- (Se-) rich films embedded in a preform and drawn into meters of fiber at a temperature well below the melting temperature of either Zn or ZnSe. By depositing 50 nm thick layers of Zn interleaved between 1 μm thick Se layers, a controlled breakup of the Zn sheet is achieved, thereby enabling a complete and controlled chemical reaction. The thermodynamics and kinetics of this synthesis process are studied using thermogravimetric analysis and differential scanning calorimetry, and the in-fiber compound is analyzed by a multiplicity of materials characterization tools, including transmission electron microscopy, Raman microscopy, energy-dispersive X-ray spectroscopy, and X-ray diffraction, all resulting in unambiguous identification of ZnSe as the compound produced from the reactive fiber draw. Furthermore, we characterize the in-fiber ZnSe/$Se_{97}S_3$ heterojunction to demonstrate the prospect of ZnSe-based fiber optoelectronic devices. The ability to synthesize new compounds during fiber drawing at nanometer scale precision and to characterize them at the atomic-level extends the architecture and materials selection compatible with multimaterial fiber drawing, thus paving the way toward more complex and sophisticated functionality.

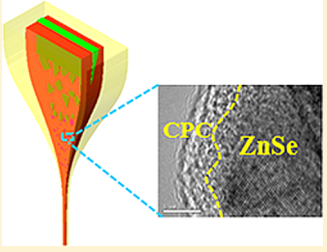

KEYWORDS: *Fiber draw synthesis, zinc selenide, TEM characterization, fiber drawing*

Preform-to-fiber drawing is a well-established process in as far as silica fibers are concerned,[1−4] and has been applied recently to other glassy materials system with the drawing of in-fiber devices for applications ranging from medical to sensing.[5−8] In its conventional form, this process is characterized by heating a preform and continuously pulling it into a fiber, thereby reducing the cross sectional dimensions while maintaining the original materials and architecture assembled in the preform. While recent work has established that disparate materials could be combined in the process, this was still limited to the materials that flow at the draw temperature. The drawing of crystalline compounds is particularly challenging as they may undergo phase separation and decompose even if they can be drawn in their liquid state. To address these challenges recent work has explored the drawing process as a new *nanocomposite synthesis tool* whereby the preform reduction zone serves the role of a chemical reaction crucible, in which materials can physically mix, chemically react, and produce new compounds that precipitate directly into the fiber.[9−12] Recent examples include the following: (1) the addition of silicon carbide powder into silicon-core/silica-clad optical fibers for purifying the Si by gettering oxygen,[10] (2) the production of silica fibers with cores comprised of the bismuth germinate family from the reaction between bismuth oxides and germanium oxides,[11] and (3) the synthesis of ZnSe from a chemical reaction at the interface between a $Se_{97}S_3$ film and a $Sn_{85}Zn_{15}$ electrode during fiber drawing.[12] Despite these proof-of-concept demonstrations, very little has been done to optimize compound synthesis, comprehensively characterize the produced compounds, or study the underlying thermodynamics and kinetics driving the chemical reactions. In this work, we demonstrate a versatile and high-throughput method for synthesizing ZnSe during a fiber draw from a scalable multilayered structure comprised of elemental solid state Zn and $Se_{97}S_3$, and provide direct atomic-level compositional and structural analysis of the produced

Received: November 1, 2012
Revised: January 11, 2013
Published: January 31, 2013

 © 2013 American Chemical Society

chemical compound. Furthermore, we experimentally probe the thermodynamics and kinetics of the in-fiber compound synthesis process. The methods described herein open a new path toward vastly expanding the set of possible materials and architectures compatible with multimaterial multifunctional fibers.

ZnSe is a widely used direct bandgap semiconductor with excellent optical and optoelectronic properties.[13−18] Recent efforts have focused on producing ZnSe structures in fibers with promising applications ranging from optical transmission to distributed photodetection.[19,20] Directly drawing ZnSe from a preform-confined melt to a fiber is complicated due to its high melting point of 1525 °C, high vapor pressure, and tendency to dissociate nonstoichiometrically.[21,22] Efforts to circumvent this problem have relied on postdraw chemical vapor deposition techniques.[19,23] Recently, it was discovered that ZnSe could be produced *in situ* during a fiber draw from the reaction of a Zn-containing electrode ($Sn_{85}Zn_{15}$) and a Se-containing thin film ($Se_{97}S_3$).[12] There, the possibility of fabricating ZnSe over scalable lengths directly during fiber drawing was demonstrated, but the methods used have two fundamental drawbacks. First, the location of the reaction was limited only to the surface of an electrode, while the bulk remained unutilized. Second, the electrode used was an alloy composed primary of another element (Sn), which had no contribution in the chemical reaction. Both significantly restrict the volume of ZnSe that can be produced and complicate characterization efforts. Here, we demonstrate a new method to synthesize ZnSe which addresses the above shortcomings. This method, based on thermal deposition of multiple alternating layers of nanoscale-thick elemental Zn and $Se_{97}S_3$, significantly increases the volume of ZnSe produced and importantly, enables unambiguous materials characterization.

Parts a and b of Figure 1 depict the details of the preform assembly and periodic multilayer architecture of the two chemical precursors necessary to form ZnSe. The multilayer Zn/$Se_{97}S_3$ structure is evaporated onto a wide conductive polycarbonate (CPC) pad which is contacted by a metal ($Sn_{63}Pb_{37}$) bus (see the Supporting Information, section 1, for details). Evaporated on the opposite side of the Zn/$Se_{97}S_3$ multilayers is a 50 μm thick, 10 mm wide $Se_{97}S_3$ film which bridges the multilayer structure to another $Sn_{63}Pb_{37}$ metal bus, forming a two-terminal circuit. The preform cladding material is polysulfone (PSU), which codraws well with $Se_{97}S_3$, CPC, and $Sn_{63}Pb_{37}$ at ∼260 °C.[24] During the draw, the Zn- and Se-rich layers mix, react, and precipitate ZnSe. Although the melting temperature of elemental Zn (420 °C)[22] exceeds the preform drawing temperature, the 50 nm thick Zn layers do not impede the draw and completely react with the Se. The wide $Se_{97}S_3$ layer and synthesized ZnSe form a heterojunction in this two-terminal circuit as will be discussed later in the text. The use of the CPC electrode allows enlarging the effective junction area while kinetically mitigating capillary breakup that would otherwise occur from the sheer flow at a liquid-metal/Se interface during the draw. The relatively low resistivity of CPC (10^2−10^6 Ω cm) also facilitates charge transport from the thin film formed on one side of the CPC pad to the metal bus on the other side.[7] The assembled structure is thermally consolidated under a pressure of 200 psi at 195 °C to form a monolithic preform, which is drawn into meters of fiber as shown in Figure 1c−e.

Post draw, atomic-level inspection at the surface of CPC where the Zn and $Se_{97}S_3$ mixed is performed using a high-resolution transmission electron microscope (HRTEM). Figure 2(a) is a micrograph of the cross section of the as-drawn fiber which shows a clear crystallized area surrounded by amorphous material. Figure 2b illustrates the fast Fourier transform (FFT) image of the marked crystalline region in Figure 2a, which indicates that the image is viewed along the ⟨011⟩ zone axis of the zincblende structure, as corroborated by comparison with the simulated diffraction pattern as shown in Figure 2c. The

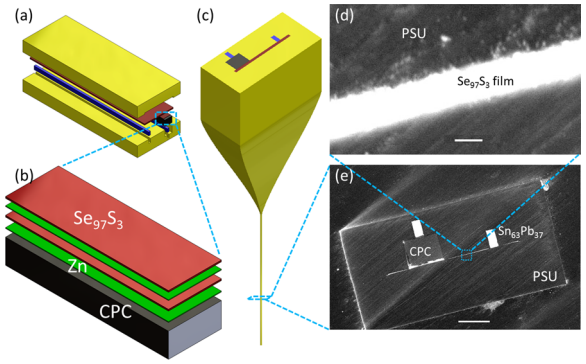

Figure 1. Preform and fiber fabrication process. (a) Schematics of the preform assembly showing the PSU cladding (yellow), CPC electrode (black), $Sn_{63}Pb_{37}$ electrodes (blue), and the $Se_{97}S_3$ film (red). (b) Zoomed-in illustration of the alternately layered $Se_{97}S_3$ (red) and Zn (green) films, which are thermally evaporated onto the CPC slab (black). Eleven layers of $Se_{97}S_3$ (1 μm each) and 10 layers of Zn (50 nm each) are evaporated in total, while the figure shows only a part of them. (c) Illustration of the thermal drawing process. (d, e) Scanning electron microscope (SEM) images of the fiber cross section. Scale bars: (d) 1 μm, (e) 200 μm.

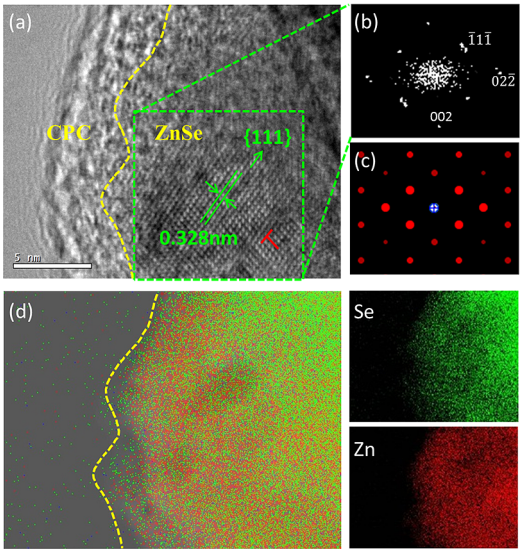

Figure 2. TEM characterization of crystallized area in amorphous surrounding (a) a high magnification TEM micrograph of crystalline ZnSe surrounded by amorphous material. The red 'T' indicates an edge dislocation. The dashed yellow curve obtained from part d indicates the boundary between CPC and ZnSe. Scale bar: 5 nm. (b) Fast Fourier transform (FFT) image of the area marked by a dashed green square in part a. (c) Simulated diffraction pattern along the [011] direction of ZnSe with zincblende structure. (d) Energy-dispersive X-ray spectroscopy (EDX) mapping of the same area in part a. Green dots represent distribution of Se, and red dots represent distribution of Zn. The dashed yellow line is the same as in part a.

dx.doi.org/10.1021/nl304023z | *Nano Lett.* 2013, 13, 975−979

two parallel lines highlighted in Figure 2(a) represent {111} planes. The spacing between the neighboring planes is 0.328 nm, from which the lattice constant of the material is calculated to be 5.68 Å. The detailed lattice structure information helps identify the crystalline material to be ZnSe (See Supporting Information, section 2, for details). An energy-dispersive X-ray spectroscopy (EDX) mapping using scanning transmission electron microscopy (STEM) as shown in Figure 2d identifies the elements present in the same area as marked in Figure 2a. This elemental distribution map shows that Zn and Se dominate in the crystalline area and that they mix uniformly at the nanoscale as shown in Figure 2d, which further supports the claim that the ZnSe compound is synthesized during the fiber draw. A point-by-point scan with TEM and EDX on different sections along the fiber axis reveals that the ZnSe islands exist randomly near the surface of CPC surrounded by Se−S. Considering all the Zn is used up in reaction with Se−S (as discussed later), the formed compound volume can be estimated to be ∼1% of total $Se_{97}S_3$. With more layers of alternating structure, the volume percentage can be further increased.

In addition to HRTEM, we also characterize the fiber using Raman spectroscopy. The Raman spectra of the thin film illustrated in Figure 3 show that two distinctly different peak

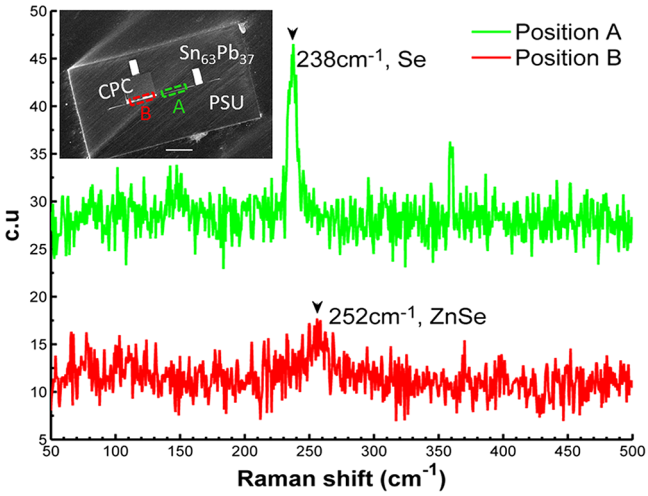

Figure 3. Raman characterization. Laser wavelength =532.17 nm, beam radius =500 nm. The red trace and green trace correspond to Raman spectra recorded from two different regions, as illustrated in the inset. Labels A and B correspond to the regions that contain only $Se_{97}S_3$ and that contain $Se_{97}S_3$ with ZnSe, respectively. Inset scale bar: 200 μm.

patterns exist at different regions along its length. In the region away from the CPC electrode where no ZnSe is expected, labeled A, all of the Raman spectra have a strong peak at 238 cm^{-1}. This is completely consistent with the Raman response of trigonal Se, which has a single strong peak at ∼237 cm^{-1} corresponding to the A_1 mode.[25,26] This is expected since the film in this region of the fiber is pure $Se_{97}S_3$. In the region directly beneath the CPC electrode where the ZnSe synthesis is expected to occur, labeled B, a different Raman distribution is measured at certain (but not all) locations (see Supporting Information, section 3, for details). A weak peak shows up at 252 cm^{-1}. This is also completely consistent with the Raman spectra of thin film ZnSe where there is essentially only one peak at 251 cm^{-1}, which corresponds to the 1LO band of ZnSe.[19,27,28] The difference in signal strength between Se and ZnSe arises from the intrinsically strong response from Se and the fact that the amount of ZnSe is much smaller than Se (see Supporting Information, section 3, for details). Comparison between these two patterns further confirms compound formation.

We proceed to discuss the mechanism by which this unique synthesis method can occur during fiber drawing. Noticing that Zn has a melting temperature of 419 °C (therefore, it is still solid at the draw temperature) and ZnSe melts at 1525 °C, it is surprising that a solid-state compound is synthesized from a solid-state precursor material in such a short time (the dwell time of the preform cone in the furnace is ∼20 min). In order to investigate how this happens, thermogravimetric analysis (TGA) and differential scanning calorimetry (DSC) are carried out on a sample comprised of alternatingly evaporated $Se_{97}S_3$/Zn layers. The thickness of the layers is the same as that in the preform, thereby mimicking the above-described structure in the preform. The heating process for both tests simulates the same fiber drawing conditions. Specifically, the material is first heated to around 270 °C, dwells for approximately 10 min, and then gets cooled down to room temperature.

During the TGA measurements, materials with a low melting temperature and high vapor pressure will be easily vaporized and those with lower vapor pressures will remain (see Supporting Information, section 4, for details). The inset of Figure 4a shows the sample before and after the TGA measurement. Before the measurement, the $Zn/Se_{97}S_3$ sample

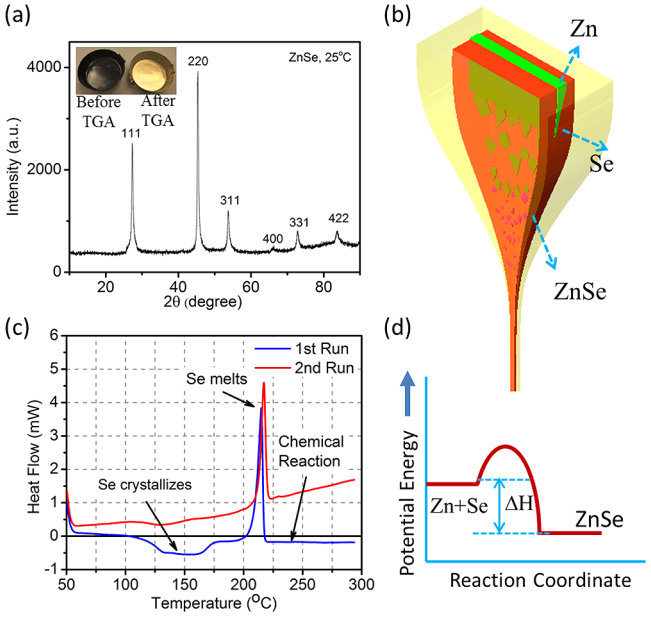

Figure 4. Thermal analysis of chemical reaction. (a) X-ray diffraction (XRD) spectrum shows that the synthesized ZnSe from the TGA test is mostly polycrystalline. Inset: image of ZnSe after TGA (right) compared with evaporated $Se_{97}S_3$ with Zn (left). (b) Schematic diagram depicting the proposed mechanism of the fiber-draw-induced chemical reaction. The Zn layer breaks up and reacts with the surrounding Se to form ZnSe compound. (c) DSC test runs twice: first run shows the process of Se crystallization and melting. The negative heat flow after the crystallization of Se indicates that an exothermic chemical reaction is taking place. However, in the second run only the Se melting peak shows up and heat flow is constantly positive. (d) Reaction diagram, showing the exothermic nature of this reaction.

dx.doi.org/10.1021/nl304023z | Nano Lett. 2013, 13, 975−979

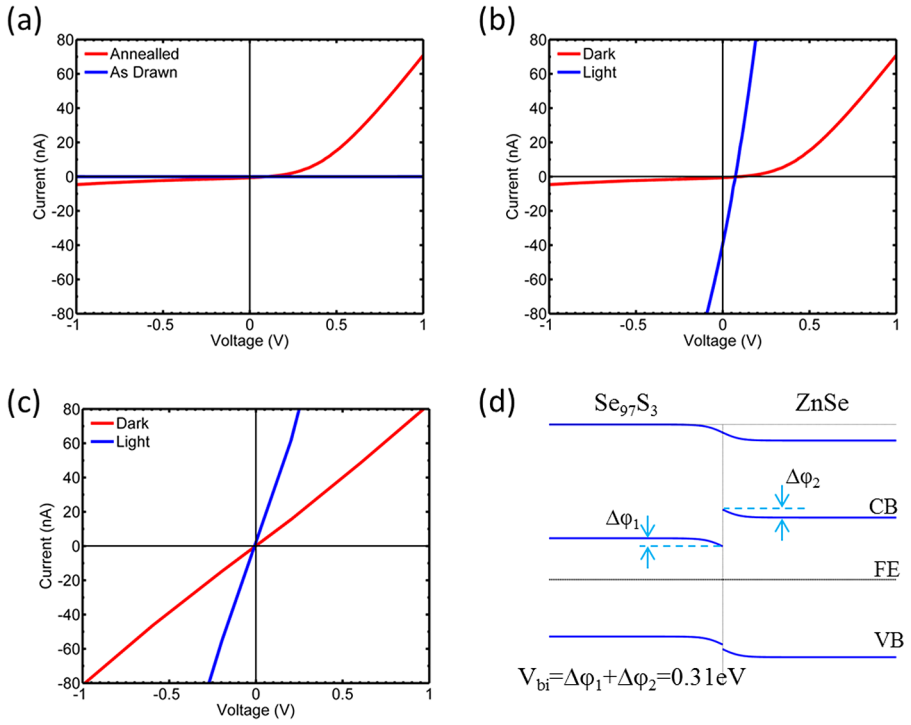

Figure 5. Optoelectronic characterization and band diagram. (a) Comparison between as-drawn fiber and fiber after annealing under dark. (b) Electrical behavior in dark and under illumination for $Se_{97}S_3$ thin film embedded with ZnSe particles indicates a rectifying junction exists in the circuit, (c) Linear $I-V$ property of pure $Se_{97}S_3$ shows the presence of an ohmic contact between $Se_{97}S_3$ and CPC, $Sn_{63}Pb_{37}$. (d) Band diagram showing that a rectifying junction is formed between $Se_{97}S_3$ and ZnSe. CB: conduction band. FE: Fermi energy. VB: valence band. V_{bi}: built-in potential.

has a dark metallic color. After the measurement, however, the material remaining in the container appears dark yellow and is identified to be polycrystalline ZnSe by X-ray diffraction (XRD) as shown in Figure 4a, indicating that a chemical reaction occurred during the measurement. The XRD measurement also reveals that ZnSe has a grain size of around 63 nm (see Supporting Information, section 5, for details). This grain size is the same order as the thickness of each Zn layer in the preform. Based on this observation, we propose the mechanism that is illustrated in Figure 4b, where the Zn layers are deformed and broken into small pieces as they flow and react with the surrounding Se fluid, precipitating out ZnSe particles. The break-up of the Zn layer is caused by the stress generated during drawing process, which is further determined by the local temperature and drawing speed. The nanometer-scale Zn thin films help achieve a thorough chemical reaction, as indicated by XRD result in Figure 4a.

DSC measurements provide independent and direct evidence of a chemical reaction between Se and Zn as they are heated. As seen from Figure 4c, in the first DSC run, two peaks show up, where the first and second peak correspond to the crystallization and melting of Se, respectively. Importantly, after the crystallization peak, the heat flow remains negative (except the melting peak of Se) despite the fact that the sample is being heated. This release of heat can only be explained by the initiation of an exothermic chemical reaction between the constituent materials, which is shown in eq 1[29] and schematically in Figure 4d.

$$\mathrm{Zn} + \mathrm{Se} = \mathrm{ZnSe}, \qquad \Delta H = -\frac{163\ \mathrm{kJ}}{\mathrm{mol}} \tag{1}$$

After the material is cooled, a second DSC run is performed on the same sample. During this second run the heat flow is always positive, which means no chemical reaction is taking place. This indicates that the synthesized compound has not decomposed and that all the Zn has been used up in the chemical reaction during the first DSC run.

The newly created compound can act as a functional component in fiber devices. Since ZnSe is a direct bandgap semiconductor with a bandgap of 2.7 eV[30] (corresponding to 459 nm), it is an attractive material for optoelectronic devices in the visible wavelength range. The fiber's optoelectronic properties are detailed in Figure 5. Prior to optoelectronic characterization, the fiber is annealed at 150 °C for 1 h in order to crystallize the wide $Se_{97}S_3$ layer. In the crystallized state, the conductivity of $Se_{97}S_3$ improves by about 8 orders of magnitude.[24,31] as depicted in Figure 5a. The current–voltage characteristics both in the dark and under illumination for the annealed sample are shown in Figure 5b. The $Sn_{63}Pb_{37}$ electrode directly contacting $Se_{97}S_3$ is forward biased. The diode-like electronic behavior in the dark suggests the existence of a built-in potential in the circuit. In contrast, a control fiber without any Zn shows a purely ohmic response, as determined from the linear $I-V$ curve depicted in Figure 5c. Comparing the distinctly different $I-V$ behaviors and using the documented electronic structure information of all the materials comprising the in-fiber circuit,[12,30,32,33] we can unambiguously ascribe the built-in potential to the ZnSe/$Se_{97}S_3$ junction (see Supporting Information, section 6, for details). The proposed band diagram for this device is shown in Figure 5d) Here, we can see that electrons are forbidden to transport through the interface of ZnSe and $Se_{97}S_3$; however, holes can easily drift from ZnSe to $Se_{97}S_3$ with the help of the built-in electric field. A built-in

dx.doi.org/10.1021/nl304023z | Nano Lett. 2013, 13, 975–979

potential of 0.31 eV is calculated based on the referenced values,[12,30,32,33] as shown in Figure 5d.

In conclusion, we demonstrate a layer-by-layer method to synthesize ZnSe *in situ* during fiber drawing and provide direct atomic-level observation and analysis of the synthesized compound. The alternating evaporation approach central to this fabrication process significantly increases product throughput and enables precise control over the reaction location inside the fiber. The methods described herein set the stage for expanding the materials and architectures possible with fiber drawing, thus paving the way toward more complex and sophisticated fiber devices.

■ ASSOCIATED CONTENT

Ⓢ Supporting Information

Detailed information of experiment and discussion of experimental results. This material is available free of charge via the Internet at http://pubs.acs.org.

■ AUTHOR INFORMATION

Corresponding Author

*E-mail: yoel@mit.edu.

Present Address

[†]QD Vision, Lexington, MA 02421

Notes

The authors declare no competing financial interest.

■ ACKNOWLEDGMENTS

We thank Dr. Yong Zhang, Timothy McClure, and Scott Speakman from CMSE and Dr. Steven Kooi, and William DiNatale from ISN for help on experiments. This work was supported in part by the Materials Research Science and Engineering Program of the US National Science Foundation (Award No. DMR-0819762) and also in part by the US Army Research Office through the Institute for Soldier Nanotechnologies (Contract No. W911NF-07-D-0004).

■ REFERENCES

(1) Senior, J. M. *Optical Fiber Communications: Principles and Practice*; Prentice Hall: Englewood Cliffs, NJ, 1985.

(2) Agrawal, G. P. *Fiber-Optic communication systems*, 3rd ed.; Wiley-Interscience: New York, 2002.

(3) Knight, J. C. *Nature* **2003**, *424* (6950), 847−851.

(4) Russell, P. *Science* **2003**, *299* (5605), 358−362.

(5) Bayindir, M.; Sorin, F.; Abouraddy, A. F.; Viens, J.; Hart, S. D.; Joannopoulos, J. D.; Fink, Y. *Nature* **2004**, *431* (7010), 826−829.

(6) Abouraddy, A. F.; Bayindir, M.; Benoit, G.; Hart, S. D.; Kuriki, K.; Orf, N.; Shapira, O.; Sorin, F.; Temelkuran, B.; Fink, Y. *Nat. Mater.* **2007**, *6* (5), 336−347.

(7) Egusa, S.; Wang, Z.; Chocat, N.; Ruff, Z. M.; Stolyarov, A. M.; Shemuly, D.; Sorin, F.; Rakich, P. T.; Joannopoulos, J. D.; Fink, Y. *Nat. Mater.* **2010**, *9* (8), 643−648.

(8) Stolyarov, A. M.; Wei, L.; Shapira, O.; Sorin, F.; Chua, S. L.; Joannopoulos, J. D.; Fink, Y. *Nat. Photonics* **2012**, *6* (4), 229−233.

(9) Snitzer, E.; Tumminelli, R. *Opt. Lett.* **1989**, *14* (14), 757−759.

(10) Morris, S.; Hawkins, T.; Foy, P.; McMillen, C.; Fan, J.; Zhu, L.; Stolen, R.; Rice, R.; Ballato, J. *Opt. Mater. Express* **2011**, *1* (6), 1141−1149.

(11) Ballato, J.; McMillen, C.; Hawkins, T.; Foy, P.; Stolen, R.; Rice, R.; Zhu, L.; Stafsudd, O. *Opt. Mater. Express* **2012**, *2* (2), 153−160.

(12) Orf, N. D.; Shapira, O.; Sorin, F.; Danto, S.; Baldo, M. A.; Joannopoulos, J. D.; Fink, Y. *Proc. Natl. Acad. Sci. U.S.A.* **2011**, *108* (12), 4743−4747.

(13) Matsuoka, T. *Adv. Mater.* **1996**, *8* (6), 469−479.

(14) Sou, I. K.; Ma, Z. H.; Wong, G. K. L. *Appl. Phys. Lett.* **1999**, *75* (23), 3707−3709.

(15) Gavrushchuk, E. M. *Inorg. Mater.* **2003**, *39* (9), 883−898.

(16) Sorokina, I. T. *Opt. Mater.* **2004**, *26* (4), 395−412.

(17) Zimmer, J. P.; Kim, S. W.; Ohnishi, S.; Tanaka, E.; Frangioni, J. V.; Bawendi, M. G. *J. Am. Chem. Soc.* **2006**, *128* (8), 2526−2527.

(18) Mirov, S.; Fedorov, V.; Moskalev, I.; Martyshkin, D.; Kim, C. *Laser Photonics Rev.* **2010**, *4* (1), 21−41.

(19) Sparks, J. R.; He, R. R.; Healy, N.; Krishnamurthi, M.; Peacock, A. C.; Sazio, P. J. A.; Gopalan, V.; Badding, J. V. *Adv. Mater.* **2011**, *23* (14), 1647−1651.

(20) Krishnamurthi, M.; Barnes, E.; Sparks, J. R.; He, R. R.; Baril, N. F.; Sazio, P. J. A.; Badding, J. V.; Gopalan, V. *Appl. Phys. Lett.* **2012**, *101*, 2.

(21) Kimura, H.; Komiya, H. *J. Cryst. Growth* **1973**, *20* (4), 283−291.

(22) Okamoto, H. *J. Phase Equilib.* **1997**, *18* (6), 676−676.

(23) He, R.; Day, T. D.; Krishnamurthi, M.; Sparks, J. R.; Sazio, P. J.; Gopalan, V.; Badding, J. V. *Adv. Mater.* **2012**, DOI: 10.1002/adma.201203879.

(24) Gumennik, A.; Stolyarov, A. M.; Schell, B. R.; Hou, C.; Lestoquoy, G.; Sorin, F.; McDaniel, W.; Rose, A.; Joannopoulos, J. D.; Fink, Y. *Adv. Mater.* **2012**, *24*, 6005−6009.

(25) Lucovsky, G. *Phys. Status Solidi B: Basic Res.* **1972**, *49* (2), 633−641.

(26) Yang, K. F.; Cui, Q. L.; Hou, Y. Y.; Liu, B. B.; Zhou, Q.; Hu, J. Z.; Mao, H. K.; Zou, G. *J. Phys.: Condens. Matter* **2007**, *19* (42), 425220.

(27) Nesheva, D.; Scepanovic, M. J.; Askrabic, S.; Levi, Z.; Bineva, I.; Popovic, Z. V. *Acta Phys. Pol., A* **2009**, *116* (1), 75−77.

(28) Taylor, W. *Phys. Lett.* **1967**, *24A* (10), 556−558.

(29) Kubaschewski, O.; Alcock, C.; Spencer, P. *Materials Thermochemistry*, 6th ed.; Pergamon Press: Oxford, U.K., 1993.

(30) Yu, P. Y.; Cardona, M. *Fundamentals of Semiconductors: Physics and Materials Properties*, 3rd ed. Springer Verlag: Berlin, 2004.

(31) Deng, D. S.; Orf, N. D.; Danto, S.; Abouraddy, A. F.; Joannopoulos, J. D.; Fink, Y. *Appl. Phys. Lett.* **2010**, *96* (2), 023102.

(32) Swank, R. K. *Phys. Rev.* **1967**, *153* (3), 844−849.

(33) Abbott, P.; Sosa, E. D.; Golden, D. E. *Appl. Phys. Lett.* **2001**, *79* (17), 2835−2837.